

Similarity states of passive scalar transport in isotropic turbulence

J. R. Chasnov^{a)}

Center for Turbulence Research, NASA Ames Research Center, Moffett Field, California 94035

(Received 23 March 1993; accepted 18 June 1993)

By simple analytical and large-eddy simulations, the time evolution of the kinetic energy and scalar variance in decaying isotropic turbulence transporting passive scalars are determined. The evolution of a passive scalar field with and without a uniform mean gradient is considered. First, similarity states of the flow during the final period of decay are discussed. Exact analytical solutions may be obtained, and these depend only on the form of the energy and scalar-variance spectra at low wave numbers, and the molecular transport coefficients. The solutions for a passive scalar field with mean-scalar gradient are of special interest, and we find that the scalar variance may grow or decay asymptotically in the final period, depending on the initial velocity distribution. Second, similarity states of the flow at high Reynolds and Péclet numbers are considered. Here it is assumed that the solutions also depend on the low-wave-number spectral coefficients, but not on the molecular transport coefficients. This results in a nonlinear dependence of the kinetic energy and scalar variance on the spectral coefficients, in contrast to the final period results. The analytical results obtained may be exact when the similarity solutions depend only on spectral coefficients that are time invariant. The present analysis also leads directly to a similarity state for a passive scalar field with uniform mean scalar gradient. Last, large-eddy simulations of the flow field are performed to test the theoretical results. Asymptotic similarity states at large times in the simulations are obtained and found to be in good agreement with predictions of the analysis. Several dimensionless quantities are also determined, which compare favorably to earlier experimental results. An argument for the inertial subrange scaling of the scalar-flux spectrum is presented, which yields a spectrum proportional to the scalar gradient and decaying as $k^{-7/3}$. This result is partially supported by the small-scale statistics of the large-eddy simulations.

I. INTRODUCTION

The most basic result in a study of homogeneous turbulence with transported scalars is the evolution of the kinetic energy and scalar variance as a function of time. Here we consider passive scalars in decaying isotropic turbulence. The passive scalar fluctuations are introduced into the turbulence in one of two ways. First, random statistically isotropic passive scalar fluctuations are introduced directly into the fluid at the initial instant of time. The introduced scalar fluctuations are then smoothed by turbulent mixing and molecular diffusion, and the scalar variance decays with the mean-square velocity. Second, a weak uniform mean scalar gradient is imposed across a turbulent fluid. Statistically homogeneous (but not isotropic) passive scalar fluctuations are then created as a consequence of the turbulent motion along the mean gradient; the scalar variance is initially zero and then increases. At later times turbulent mixing and molecular diffusion act to smooth the generated scalar fluctuations.

Experimentally, decaying isotropic turbulence is approximated by grid-generated turbulence and the decay of the turbulence with distance from the grid corresponds to the decay in time of an isotropic turbulence. Experiments on grid-generated turbulence with and without passive scalars are numerous, and interested readers can refer to Refs.

1–4 for additional details and references. At the moderate Reynolds numbers attainable in grid-turbulence facilities, it has been determined that the kinetic energy in isotropic turbulence decays asymptotically in time as a power law; Comte-Bellot and Corrsin¹ find the decay to be approximately $t^{-1.25}$ and Warhaft and Lumley³ find $t^{-1.34}$. Isotropic passive scalar fluctuations, introduced into decaying grid-generated turbulence by weakly heating the grid or by placing a heated mesh of wires downstream from an unheated grid, likewise decays in time, but the power-law exponent is less certain. Warhaft and Lumley³ determined that the experimental uncertainty is due to the measured exponent being a function of the ratio between the initial integral length scales of the velocity and scalar fluctuations. In a different but related study of decaying isotropic turbulence in the presence of a passive mean scalar gradient, Sirivat and Warhaft⁴ determined that the passive scalar variance increases approximately linearly in time at large times.

The idea of a power-law decay of the kinetic energy seems to be widely accepted (although the exact exponent is less certain), but the behavior of the passive scalar variance is still controversial. After the experimental data of Warhaft and Lumley³ was published, theoretical arguments were proposed,^{5–7} suggesting that the scalar-variance decay laws measured in the experiments are of a transient nature, and that for sufficiently high Reynolds and Péclet numbers and long times, a universal value for the power-law exponent of the decay would be found.

^{a)}Present address: The Hong Kong University of Science and Technology, Clear Water Bay, Kowloon, Hong Kong.

However, recent large-eddy simulations^{8,9} have brought these latter theoretical results into question, although additional closure calculations¹⁰ indicate that the numerical flow fields may not be evolved sufficiently. The time evolution of the scalar variance in the presence of a passive mean scalar gradient has received somewhat less theoretical attention because of the analytical difficulties in treating an anisotropic scalar field, although here we mention the original theoretical work of Corrsin,¹¹ who noted the constancy of a uniform mean scalar gradient, and the more recent closure and numerical simulation studies by Sanderson *et al.*,¹² whose results are in reasonable agreement with those of the Sirivat and Warhaft experiment.

In this paper we study, in detail, by simple analytic means and by large-eddy numerical simulations, the evolution of the mean-square velocity and passive scalar variance in decaying isotropic turbulence. The results we obtain for the decay of the mean-square velocity and the scalar variance without mean scalar gradient are known,¹³ although our derivation differs somewhat from earlier work and more closely follows the spirit of a recent paper¹⁴ on homogeneous buoyancy-generated turbulence. Our argument is also easily extended to determine a new similarity state for the asymptotic evolution of the scalar field with mean passive scalar gradient.

We also present the results of new large-eddy simulations of 256³ resolution in which the numerical flow fields are evolved sufficiently long in time to determine approximate asymptotic decay laws of both the kinetic energy and scalar variance with and without a mean scalar gradient. Large-eddy simulations appear to be uniquely suited for this problem: the large-scale statistics of interest are insensitive to the exact form of the subgrid scale model and alternative approaches, such as physical experiments and direct numerical simulations are too severely restricted in Reynolds and Péclet number and total flow evolution time to precisely test the theoretical predictions. Closure calculations can attain the high Reynolds numbers and long-time evolutions of interest here,¹³ but contain unknown errors that can be quantified only by comparison to numerical simulation.

II. THE GOVERNING EQUATIONS

The relevant equations for isotropic turbulence convecting a passive scalar field with or without a mean scalar gradient are

$$\nabla \cdot \mathbf{u} = 0, \quad (1)$$

$$\frac{\partial \mathbf{u}}{\partial t} + \mathbf{u} \cdot \nabla \mathbf{u} = -\frac{\nabla p}{\rho_0} + \nu \nabla^2 \mathbf{u}, \quad (2)$$

$$\frac{\partial \theta}{\partial t} + \mathbf{u} \cdot \nabla \theta = -\beta u_3 + D \nabla^2 \theta, \quad (3)$$

where p and \mathbf{u} are the fluid pressure and velocity, θ is the passive scalar field, ν is the kinematic viscosity, and D is the molecular diffusivity of the scalar. The fluid is taken to be infinite in all directions and the averaged properties of the velocity and scalar field are assumed to be independent

of position. In (3), β is the constant mean scalar gradient taken without loss of generality to be in the x_3 direction. The cases $\beta=0$ and $\beta \neq 0$ will be considered separately.

III. THE FINAL PERIOD OF DECAY

Exact analytical treatment of (1)–(3) is rendered difficult because of the quadratic terms. Under conditions of a final period of decay¹⁵ these terms may be neglected, and an analytical solution of (1)–(3) may be determined. Although most of the final period results are well known,¹⁶ we recall them here since the ideas that arise in a consideration of the final period will be relevant to our high Reynolds number analysis.

During the final period, viscous and diffusive effects dissipate the high-wave-number components of the energy and scalar-variance spectra, and at late times the only relevant part of the spectra are their forms at small wave numbers. Defining the energy spectrum $E(k,t)$ and the passive scalar-variance spectrum $E_\theta(k,t)$ to be the spherically integrated three-dimensional Fourier transform of the covariances $\frac{1}{2}\langle u_i(\mathbf{x},t)u_i(\mathbf{x}+\mathbf{r},t) \rangle$ and $\frac{1}{2}\langle \theta(\mathbf{x},t)\theta(\mathbf{x}+\mathbf{r},t) \rangle$, where $\langle \dots \rangle$ denotes an ensemble or volume average, expansions of the spectra near $k=0$ can be written as

$$E(k,t) = 2\pi k^2 (B_0 + B_2 k^2 + \dots), \quad (4)$$

$$E_\theta(k,t) = 2\pi k^2 (C_0 + C_2 k^2 + \dots), \quad (5)$$

where B_0, B_2, \dots , and C_0, C_2, \dots , are the Taylor series coefficients of the expansion. When the Taylor series do not converge, (4) and (5) should be considered as lowest-order asymptotic expansions. Under the assumption that all the Taylor series coefficients of (4) converge at the initial instant, Batchelor and Proudman¹⁷ determined that $B_0=0$, and that nonlinear interactions (which are important during the initial period) necessarily result in a time-dependent nonzero value of B_2 and the divergence of the remaining Taylor series coefficients. Saffman¹⁸ later showed that if the turbulence was created by a nonsolenoidal impulsive body force per unit mass applied to the fluid at the initial instant, then B_2 and higher-order coefficients diverge, but B_0 is finite and nonzero and is invariant in time throughout the evolution of the flow. In the absence of a mean scalar gradient ($\beta=0$), C_0 is invariant during the entire evolution of the flow,¹⁹ and for special initial conditions such that $C_0=0$, nonlinear interactions generate a finite, nonzero, time-dependent value for C_2 .

For $\beta \neq 0$, an exact relationship between C_0 and B_0 may be obtained directly from the governing equations. The equation for the evolution of the mean of the product of $\theta(\mathbf{x})$ and $\theta(\mathbf{x}')$ obtained from (3) is

$$\frac{\partial \langle \theta \theta' \rangle}{\partial t} = \nabla_r \cdot \langle \mathbf{u} \theta \theta' - \mathbf{u}' \theta \theta' \rangle + 2D \nabla_r^2 \langle \theta \theta' \rangle - \frac{\beta}{2} \langle u_3 \theta' + u_3' \theta \rangle, \quad (6)$$

where θ and θ' stand for $\theta(\mathbf{x})$ and $\theta(\mathbf{x}')$ and $\mathbf{r}=\mathbf{x}'-\mathbf{x}$. Defining the spectrum of the vertical scalar flux $F(k,t)$ to be the spherically integrated three-dimensional Fourier

transform of the covariance $\langle u_3(\mathbf{x},t)\theta(\mathbf{x}+\mathbf{r},t) \rangle$, an asymptotic expansion of $F(k,t)$ near $k=0$ may be written as

$$F(k,t) = 4\pi k^2 (A_0 + A_2 k^2 + \dots). \quad (7)$$

Taking the three-dimensional Fourier transform of (6) and setting $k=0$, one obtains

$$\frac{dC_0}{dt} = -\beta A_0, \quad (8)$$

under the reasonable assumption that the Fourier transform of the third-order two-point product of u and θ is regular at $k=0$. Note that when $\beta=0$, (8) is simply a statement of the invariance of C_0 . An equation for A_0 may be similarly derived from the three dimensional Fourier transform of the expression for the rate of change of $\langle u_3\theta' + u_3'\theta \rangle/2$ evaluated at $k=0$:

$$\frac{dA_0}{dt} = -\frac{\beta}{3} B_0, \quad (9)$$

where use has been made of the isotropy of the velocity statistics. Equations (8) and (9) may be integrated directly since B_0 is independent of time, and at large times one finds

$$C_0(t) = \frac{1}{3}\beta^2 B_0 t^2. \quad (10)$$

This result is exact for all times if there are initially no scalar fluctuations.

During the final period of decay, when interactions between different wave number components of the velocity and scalar fields are negligible, the leading coefficient B_2 is independent of time, as is C_2 when $\beta=0$. For $\beta \neq 0$, C_2 evolves asymptotically during the final period as

$$C_2 = \frac{1}{3}\beta^2 B_2 t^2. \quad (11)$$

We digress for a moment to show how a general type of scalar and velocity distribution can be seen to correspond to nonzero values of C_0 and B_0 . By definition, C_0 is equal to

$$C_0 = \frac{1}{8\pi^3} \int \langle \theta(\mathbf{x},t)\theta(\mathbf{x}+\mathbf{r},t) \rangle d\mathbf{r}. \quad (12)$$

Statistical homogeneity of the flow implies the equivalence of spatial averages and ensemble mean values and the independence of statistical averages on position, so that (12) can be rewritten as

$$C_0 = \frac{1}{8\pi^3} \lim_{V \rightarrow \infty} \frac{1}{V} \left(\int_V \theta(\mathbf{x},t) d\mathbf{x} \right)^2 = \lim_{V \rightarrow \infty} \frac{V}{8\pi^3} \langle \theta \rangle_V^2, \quad (13)$$

where $\langle \dots \rangle_V$ now denotes an average over the finite volume V . The θ field denotes the fluctuation of the scalar quantity from its mean value, so that $\langle \theta \rangle$ is necessarily zero when the average is taken over an infinite volume. However, C_0 may have a nonzero limit if the average of θ over a finite volume decreases as $1/\sqrt{V}$ for large V . For instance, if the initial scalar distribution is such that $\theta(\mathbf{x},0)$ is independently assigned random values from a Gaussian distribution (with zero mean and variance θ_0^2) in different

regions of the fluid of volume v small compared to the total volume V , then C_0 is found to be independent of V and equal to

$$C_0 = \frac{1}{8\pi^3} v \theta_0^2. \quad (14)$$

The equation analogous to (13) for the low-wave-number energy spectral coefficient is

$$B_0 = \lim_{V \rightarrow \infty} \frac{V}{8\pi^3} (\langle u_1 \rangle_V^2 + \langle u_2 \rangle_V^2 + \langle u_3 \rangle_V^2), \quad (15)$$

so that B_0 has a nonzero limit if the average over a finite volume V for, at least, a single component of \mathbf{u} decreases as $1/\sqrt{V}$ for large V . We also note that in flows with active scalars, an initial nonzero value of C_0 directly results in an energy spectrum with nonzero value of B_0 as a direct consequence of the buoyancy force.¹⁴

Returning again to the final period of decay, the solution of (1)–(3) without the quadratic terms most easily proceeds in Fourier space, and upon use of (4) and (5) and an assumption of large times in the flow evolution one obtains, for the decay of the mean-square velocity fluctuation,

$$\langle u^2 \rangle = 4\pi [J_0 B_0 (vt)^{-3/2} + J_2 B_2 (vt)^{-5/2} + \dots], \quad (16)$$

where

$$J_0 = \int_0^\infty \eta^2 \exp(-2\eta^2) d\eta = \frac{1}{8} \sqrt{\frac{\pi}{2}},$$

$$J_2 = \int_0^\infty \eta^4 \exp(-2\eta^2) d\eta = \frac{3}{32} \sqrt{\frac{\pi}{2}}.$$

The $t^{-5/2}$ decay law was determined by Batchelor¹⁵ and the $t^{-3/2}$ decay law was determined by Saffman.¹⁸

The results obtained for the decay of an isotropic passive scalar are completely analogous. With $\beta=0$ in (3), one finds

$$\langle \theta^2 \rangle = 4\pi [J_0 C_0 (Dt)^{-3/2} + J_2 C_2 (Dt)^{-5/2} + \dots]. \quad (17)$$

The analysis for a passive scalar field with uniform mean scalar gradient is only slightly more complicated, and one finds at large times the leading-order terms

$$\langle \theta^2 \rangle = \frac{4\pi\sigma^2 I_0}{3(1-\sigma)^2} \beta^2 B_0 v^{-3/2} t^{1/2} \quad (18)$$

and

$$\langle \theta^2 \rangle = \frac{4\pi\sigma^2 I_2}{3(1-\sigma)^2} \beta^2 B_2 v^{-5/2} t^{-1/2}, \quad (19)$$

when B_0 and B_2 are the leading-order spectral coefficients, respectively, and where $\sigma = \nu/D$ is a Schmidt or Prandtl number, and

$$I_0(\sigma) = \int_0^\infty \eta^{-2} \left[\exp(-\eta^2) - \exp\left(\frac{-\eta^2}{\sigma}\right) \right]^2 d\eta,$$

$$I_2(\sigma) = \int_0^\infty \left[\exp(-\eta^2) - \exp\left(\frac{-\eta^2}{\sigma}\right) \right]^2 d\eta.$$

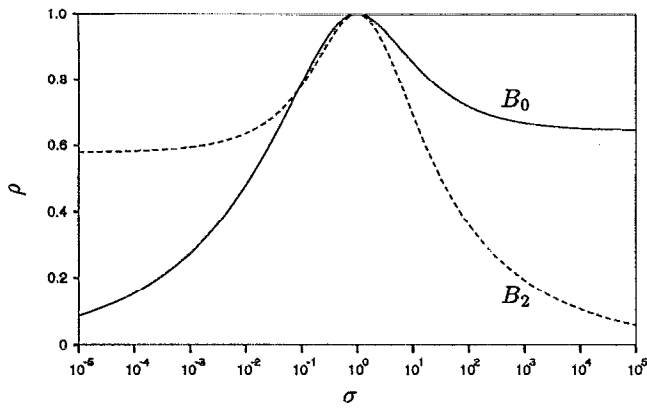


FIG. 1. The asymptotic value of the normalized correlation coefficient ρ between the scalar field and the vertical velocity fluctuation during the final period as a function of the Prandtl number σ .

The flux $\langle u_3\theta \rangle$ is nonzero for this anisotropic flow, and one finds asymptotically in the final period the corresponding solutions,

$$\langle u_3\theta \rangle = \frac{-4\pi\sigma L_0}{3(1-\sigma)} \beta B_0 \nu^{-3/2} t^{-1/2} \quad (20)$$

and

$$\langle u_3\theta \rangle = \frac{-4\pi\sigma L_2}{3(1-\sigma)} \beta B_2 \nu^{-5/2} t^{-3/2}, \quad (21)$$

where

$$L_0(\sigma) = \int_0^\infty \exp(-\eta^2) \left[\exp(-\eta^2) - \exp\left(\frac{-\eta^2}{\sigma}\right) \right] d\eta,$$

$$L_2(\sigma) = \int_0^\infty \eta^2 \exp(-\eta^2) \left[\exp(-\eta^2) - \exp\left(\frac{-\eta^2}{\sigma}\right) \right] d\eta.$$

The normalized correlation coefficient between the scalar field and the vertical velocity fluctuation, defined as

$$\rho = \frac{-\langle u_3\theta \rangle}{\langle u_3^2 \rangle^{1/2} \langle \theta^2 \rangle^{1/2}}, \quad (22)$$

approaches a time-independent value during the final period equal to

$$\rho(\sigma) = \frac{|L_0|}{\sqrt{I_0 J_0}}; \quad \rho(\sigma) = \frac{|L_2|}{\sqrt{I_2 J_2}}, \quad (23)$$

when B_0 and B_2 are the leading-order spectral coefficients, respectively. In Fig. 1, we plot the asymptotic value of ρ as a function of σ for the two possible final period flows. We note that for $\sigma=1$, the scalar and vertical velocity field become perfectly correlated with opposite sign.

The final period decay of $\langle \theta^2 \rangle$ when B_2 is the leading-order low-wave-number coefficient was obtained previously by Dunn and Reid,²⁰ who, for historical reasons, did not consider the case of nonzero B_0 . Comparing (18) and (19) to (17), one observes that $\langle \theta^2 \rangle$ decays less slowly by a factor of t^2 when $\beta \neq 0$ than when $\beta = 0$. The extra factor of t^2 arises directly from the increase in time of the low-wave-number coefficients of the scalar-variance spectrum

[see (10) and (11)]. This factor of t^2 results in an increase in $\langle \theta^2 \rangle$ during the final period when B_0 is the leading-order spectral coefficient and a decrease in $\langle \theta^2 \rangle$ when B_2 is the leading-order coefficient. The behavior of a passive scalar in the final period of grid-generated turbulence with mean scalar gradient thus provides a sensitive experimental test between a k^2 or k^4 low-wave-number energy spectrum. Previous experimental measurements^{21,22} of $\langle u^2 \rangle$ during the final period of decay in grid-generated turbulence find a $t^{-5/2}$ decay law, which implies $B_0=0$, although such experimental measurements are made difficult by the small signal to noise ratio.

The final period of decay results can also be found directly by a dimensional analysis, and we now present this alternative approach, since it will be needed at high Reynolds and Péclet numbers when exact analytical solutions cannot be determined. Linear equations govern the final period so that the dependence of $\langle u^2 \rangle$ on the low-wave-number coefficients of the energy spectrum is necessarily linear. Viscosity and time are the only other relevant dimensional parameters, so that a dimensional analysis based on $[B_0]=l^2 t^{-2}$ and $[B_2]=l^7 t^{-2}$ results in

$$\langle u^2 \rangle \propto B_0 \nu^{-3/2} t^{-3/2}, \quad \langle u^2 \rangle \propto B_2 \nu^{-5/2} t^{-5/2},$$

when B_0 and B_2 are the leading-order energy spectrum coefficients, respectively. Similar reasoning with $[C_0]=\theta^2 l^3$ and $[C_2]=\theta^2 l^5$ yields (for $\beta=0$)

$$\langle \theta^2 \rangle \propto C_0 D^{-3/2} t^{-3/2}, \quad \langle \theta^2 \rangle \propto C_2 D^{-5/2} t^{-5/2},$$

when C_0 and C_2 are the leading-order scalar-variance spectrum coefficients, respectively. For $\beta \neq 0$, C_0 may be replaced by (10) and C_2 may be replaced by (11), yielding the results of (18) and (19). Determination of numerical factors, and factors of σ when $\beta \neq 0$, apparently requires exact analytical solution of the equations.

IV. EXACT HIGH REYNOLDS NUMBER SIMILARITY STATES

At high Reynolds and Péclet numbers, direct effects of viscosity and diffusivity occur at much larger wave number magnitudes than those scales that contain most of the energy and scalar variance, so that the asymptotic forms of $\langle u^2 \rangle$ and $\langle \theta^2 \rangle$ can be expected to be independent of ν and D . Viscous and diffusive smoothing of the energy and scalar-variance containing components of the spectra are now replaced by nonlinear transfer processes, so that one can still reasonably expect the asymptotic scaling of $\langle u^2 \rangle$ and $\langle \theta^2 \rangle$ to depend on the form of the spectra at low wave numbers. The low-wave-number coefficient B_0 is an invariant, even at high Reynolds numbers, and so is C_0 if $\beta=0$. If $\beta \neq 0$, C_0 is asymptotically related to B_0 by (10).

We can now determine the high Reynolds and Péclet number, long-time evolution of the energy, and scalar variance when B_0 and C_0 are nonzero. Assuming that $\langle u^2 \rangle$ depends on the invariant B_0 and t alone, one finds directly from a dimensional analysis,

$$\langle u^2 \rangle \propto B_0^{2/5} t^{-6/5}. \quad (24)$$

The nonlinearity of the equations is reflected by the nonlinear dependence of $\langle u^2 \rangle$ on B_0 , in contrast to the results for the final period. For an isotropic scalar field with $\beta=0$, the scalar variance is assumed to be a function of the invariants C_0 and B_0 , and t alone, and dimensional analysis yields

$$\langle \theta^2 \rangle \propto C_0 B_0^{-3/5} t^{-6/5}. \quad (25)$$

The linearity of the scalar equation in θ is reflected in the linear dependence of $\langle \theta^2 \rangle$ on C_0 while the quadratic term results in a nonlinear dependence on B_0 . When $\beta \neq 0$, C_0 depends on B_0 asymptotically as (10), and the scalar variance then evolves as

$$\langle \theta^2 \rangle \propto \beta^2 B_0^{2/5} t^{4/5}, \quad (26)$$

and the vertical scalar flux evolves as

$$\langle u_3 \theta \rangle \propto \beta B_0^{2/5} t^{-1/5}. \quad (27)$$

Dimensional arguments can also determine the asymptotic behavior of the integral scales, and one finds

$$L_u, L_\theta \propto B_0^{1/5} t^{2/5}. \quad (28)$$

Dimensional arguments are insufficient to determine dimensionless quantities such as ρ , (22), when $\beta \neq 0$, and L_u/L_θ . The Reynolds and Péclet number of the turbulence—formed by the product of the root-mean-square velocity of the fluid and the integral length scale at time t , divided by the constant kinematic viscosity or diffusivity, respectively—decays as $t^{-1/5}$, so that they do not remain large indefinitely. Nevertheless, we expect the above asymptotic state to hold over intermediate times, which are long with respect to the initial instant of turbulence generation, but short with respect to a significant Reynolds or Péclet number decay.

The $t^{-6/5}$ decay law for $\langle u^2 \rangle$ was first obtained by Saffman,²³ following earlier work of Kolmogorov,²⁴ by assuming a self-similar decay of the energy spectrum, and the $t^{-6/5}$ decay law for $\langle \theta^2 \rangle$ was obtained⁵ under an analogous assumption of self-similar decay of the scalar-variance spectrum. (These arguments can also be found in Ref. 13.) The dimensional arguments presented here necessarily leads to a self-similar decay of the energy spectrum of the form

$$E(k,t) = B_0^{3/5} t^{-4/5} \hat{E}(\hat{k}), \quad \hat{k} = B_0^{1/5} t^{2/5} k, \quad (29)$$

and a self-similar decay of the scalar-variance spectrum (for $\beta=0$) of the form

$$E_\theta(k,t) = B_0^{-2/5} C_0 t^{-4/5} \hat{E}_\theta(\hat{k}), \quad \hat{k} = B_0^{1/5} t^{2/5} k, \quad (30)$$

and when $\beta \neq 0$, of the form

$$E_\theta(k,t) = \beta^2 B_0^{3/5} t^{6/5} \hat{E}_\theta(\hat{k}), \quad \hat{k} = B_0^{1/5} t^{2/5} k. \quad (31)$$

In the flow with a mean passive scalar gradient, the spectrum of the vertical scalar flux $F(k,t)$ is nonzero and has the self-similar form

$$F(k,t) = \beta B_0^{3/5} t^{6/5} \hat{F}(\hat{k}), \quad \hat{k} = B_0^{1/5} t^{2/5} k. \quad (32)$$

Thus we have found the interesting result that the scalar variance increases in time as $t^{4/5}$ in a decaying high

Reynolds number isotropic turbulence when B_0 is the leading-order spectral coefficient. Sirivat and Warhaft⁴ estimate the increase in $\langle \theta^2 \rangle$ to be linear in their experiment, although there is considerable scatter in their data, and large-eddy simulations presented in Sec. VIII will be seen to support (26).

V. APPROXIMATE HIGH REYNOLDS NUMBER SIMILARITY STATES

When B_0 or C_0 are zero, there are no longer strictly invariant quantities on which to base asymptotic similarity states. The coefficients B_2 and C_2 are determined by nonlinear transfer processes and exact analytical results as found above are unobtainable. Nevertheless, if we make the additional assumption that the time variation of B_2 is small compared to the rate of the energy decay,¹ and when $\beta=0$ the time variation of C_2 is small compared to the rate of the scalar-variance decay, then approximate asymptotic similarity states can be based on B_2 and C_2 . Closure calculations¹³ support the assumption of a slow variation in B_2 and C_2 at high Reynolds and Péclet numbers. For $\beta \neq 0$, the relevant assumption on C_2 is the approximate validity of (11).

By dimensional arguments, one then obtains, when $B_0=0$,

$$\langle u^2 \rangle \propto B_2^{2/7} t^{-10/7}. \quad (33)$$

When $\beta=0$, the scalar variance may follow the three approximate decay laws,

$$\langle \theta^2 \rangle \propto C_2 B_0^{-1} t^{-2}, \quad (34)$$

$$\langle \theta^2 \rangle \propto C_0 B_2^{-3/7} t^{-6/7}, \quad (35)$$

$$\langle \theta^2 \rangle \propto C_2 B_2^{-5/7} t^{-10/7}, \quad (36)$$

depending on which of B_0 or C_0 are zero. When $\beta \neq 0$, the scalar variance follows:

$$\langle \theta^2 \rangle \propto B_2^{2/7} t^{4/7}, \quad (37)$$

and the vertical scalar flux follows:

$$\langle u_3 \theta \rangle \propto \beta B_2^{2/7} t^{-3/7}. \quad (38)$$

The integral scales depend only on the low-wave-number coefficient of the energy spectrum, so that

$$L_u, L_\theta \propto B_2^{1/7} t^{2/7}. \quad (39)$$

The Reynolds and Péclet numbers decay as $t^{-3/7}$.

The decay law (33) was originally proposed by Kolmogorov²⁴ under the assumption of the invariance of the Loisantski integral²⁵ later shown to be equivalent to the invariance of B_2 .²⁶ Following the work of Kolmogorov, Corrsin¹⁹ assumed the invariance of B_2 and C_0 and derived the $t^{-6/7}$ decay law (35). The complete set of approximate decay laws for $\langle \theta^2 \rangle$ with $\beta=0$ were written down by Larcheveque *et al.*,⁵ and are also extensively discussed in Lesieur.¹³ When $\beta \neq 0$, the scalar variance is again seen to increase in time.

Approximate self-similar forms for the spectra may be determined when B_0 or C_0 are zero, and we record them here for later use:

$$E(k,t) = B_2^{3/7} t^{-8/7} \hat{E}(\hat{k}), \quad \hat{k} = B_2^{1/7} t^{2/7} k, \quad (40)$$

and when $\beta=0$,

$$E_\theta(k,t) = B_0^{-4/5} C_2 t^{-8/5} \hat{E}_\theta(\hat{k}), \quad \hat{k} = B_0^{1/5} t^{2/5} k, \quad (41)$$

$$E_\theta(k,t) = B_2^{-2/7} C_0 t^{-4/7} \hat{E}_\theta(\hat{k}), \quad \hat{k} = B_2^{1/7} t^{2/7} k, \quad (42)$$

$$E_\theta(k,t) = B_2^{-4/7} C_2 t^{-8/7} \hat{E}_\theta(\hat{k}), \quad \hat{k} = B_2^{1/7} t^{2/7} k. \quad (43)$$

For $\beta \neq 0$, we have

$$E_\theta(k,t) = \beta^2 B_2^{3/7} t^{6/7} \hat{E}_\theta(\hat{k}), \quad \hat{k} = B_2^{1/7} t^{2/7} k, \quad (44)$$

$$F(k,t) = \beta B_2^{3/7} t^{-1/7} \hat{F}(\hat{k}), \quad \hat{k} = B_2^{1/7} t^{2/7} k. \quad (45)$$

Lesieur and Schertzer²⁷ numerically solved the eddy-damped quasinormal Markovian (EDQNM) two-point closure equations for the energy decay in an isotropic turbulence to test the approximate validity of the Kolmogorov decay law (33) and the spectral similarity form (40). They determined that within the EDQNM closure, the energy spectrum does indeed follow the similarity form given by (40) (neglecting viscous effects), but with B_2 depending explicitly on time asymptotically as

$$B_2(t) \propto t^\gamma. \quad (46)$$

The corrected energy decay law was then determined to be

$$\langle u^2 \rangle \propto t^{-10/7+2\gamma/7}, \quad (47)$$

where Lesieur and Schertzer computed $\gamma=0.16$ using the EDQNM approximation, so that $\langle u^2 \rangle \propto t^{-1.38}$ instead of $t^{-1.43}$. We note that the precise value of γ is dependent on the arbitrary choice of the eddy-damping function in the EDQNM model, while the existence of the self-similar solution (40) only requires a choice of eddy-damping function that introduces no additional dimensional parameters into the problem.

Chollet²⁸ performed further EDQNM closure calculations for the decay of an isotropic passive scalar-variance spectrum. He determined that when B_2 and C_2 are both the leading-order coefficients in the energy and scalar-variance spectral expansions, the scalar-variance spectrum decays self-similarly as (43), where now, in addition to (46), C_2 evolves asymptotically as

$$C_2(t) \propto t^{\gamma'}. \quad (48)$$

The corrected scalar-variance decay law for this case is then

$$\langle \theta^2 \rangle \propto t^{-10/7-5\gamma/7+\gamma'}, \quad (49)$$

where Chollet determined $\gamma'=0.06$, so that $\langle \theta^2 \rangle \propto t^{-1.48}$ instead of $t^{-1.43}$. Again, the precise value of γ' is dependent on the choice of eddy-damping functions. The decay law for the scalar variance when B_2 and C_0 are the leading-order coefficients contains only the correction due to γ , and with $\gamma=0.19$ one finds a $t^{-0.93}$ decay law instead of $t^{-0.86}$. We have independently confirmed the above-mentioned

EDQNM closure computations, and have also determined a self-similar decay of the passive scalar-variance spectrum when B_0 and C_2 are the leading-order spectral coefficients. With the same eddy-damping parametrization as used by Chollet, we find

$$C_2(t) \propto t^{\gamma''}, \quad (50)$$

where $\gamma''=0.14$, approximately a factor of 2 larger than the value of γ' . This results in a $t^{-1.86}$ decay law for the scalar variance rather than t^{-2} .

A correction to the scalar-variance growth in the presence of a mean scalar gradient when B_2 is the leading-order spectral coefficient may be determined by assuming a self-similar form (neglecting viscous and diffusive effects) for the scalar-variance spectrum. If we assume that C_2 now increases asymptotically as $C_2 \propto t^{2+\gamma+\gamma''}$ as a result of the time dependence of B_2 , as represented by γ and nonlinear transfer in the scalar equation as represented by γ'' , then the scalar variance is now found to evolve asymptotically as $\langle \theta^2 \rangle \propto t^{4/7+2\gamma/7+\gamma''}$. An EDQNM computation of γ'' has not yet been performed, but it is reasonable to expect its value to be of similar order of magnitude as γ' and γ'' .

Finally, we mention a recent paper,²⁹ which revisited the consequences of assuming a complete self-similar decay of the energy spectrum.¹⁶ This is in contrast to the self-similar decay discussed above, which is only valid for scales in which the effects of viscosity may be neglected. Complete self-similar decay may take place as $t \rightarrow \infty$, only if an asymptotic expansion of the energy spectrum near $k=0$ has the peculiar form

$$E(k) = Ak + \dots$$

A dimensional analysis based on the invariant A and t yields the long-time behaviors,

$$\langle u^2 \rangle \propto A^{1/2} t^{-1}, \quad L_u \propto A^{1/4} t^{1/2},$$

for the evolution of the mean-square velocity and the integral scale of the turbulence. The corresponding Reynolds number of the flow is seen to be independent of time, as is necessary for complete self-similar decay.

VI. LARGE-EDDY SIMULATIONS

In this section, we present results of several large-eddy simulations designed to test the high Reynolds and Péclet number asymptotic scalings of Secs. IV and V. We employ a pseudospectral code for turbulence in a periodic box³⁰ with a subgrid scale model to solve directly (1)–(3). Similar numerical simulations have already been successfully performed by Batchelor *et al.*¹⁴ for homogeneous buoyancy-generated turbulence, and these simulations follow the spirit of earlier simulations performed by Lesieur and Rogallo.⁸ For the subgrid scale model, we employ a spectral eddy viscosity and eddy diffusivity,^{31,32} parametrized by

$$v_e(k|k_m, t) = \left[0.145 + 5.01 \exp\left(\frac{-3.03k_m}{k}\right) \right] \times \left(\frac{E(k_m, t)}{k_m}\right)^{1/2} \quad (51)$$

and

$$D_e(k|k_m, t) = \frac{v_e(k|k_m, t)}{\sigma_e}, \quad (52)$$

where k_m is the maximum wave number magnitude of the simulation and σ_e is an eddy Schmidt (or Prandtl) number, assumed here to be constant and equal to 0.6. Our results are insensitive to the precise values of the coefficients used in (51) and (52). The value of the molecular Schmidt number of the fluid is arbitrary, since we do not resolve either viscous or diffusive scales. We take the initial energy spectrum of the isotropic turbulence to be

$$E(k, 0) = \frac{1}{2} A_s u_0^2 k_p^{-1} \left(\frac{k}{k_p}\right)^s \exp\left[-\frac{1}{2} s \left(\frac{k}{k_p}\right)^2\right], \quad (53)$$

where s is equal to 2 or 4, A_s is given by

$$A_s = \sqrt{\frac{2}{\pi}} \frac{s^{(1/2)(s+1)}}{1 \cdot 3 \cdot \dots \cdot (s-1)}, \quad (54)$$

and k_p is the wave number at which the initial energy spectrum is maximum. The leading-order coefficient of the expansion of $E(k)$ near $k=0$ when $s=2$ or 4 is

$$B_0 = \frac{A_2 u_0^2}{4\pi k_p^3}, \quad B_2 = \frac{A_4 u_0^2}{4\pi k_p^5}, \quad (55)$$

respectively. In the 256^3 numerical simulations presented here, we take the initial root-mean-square velocity u_0 equal to unity and $k_p=100$, where the minimum computational wave number is unity (corresponding to a periodic box of length 2π), and the maximum wave number is 120. The initial energy spectrum is set to zero for wave numbers greater than 118 to allow the subgrid scale eddy viscosity and eddy diffusivity to build up from zero values. We choose as large a value of k_p as possible in an effort to attain an asymptotic similarity state before the integral scales of the flow become comparable to the periodicity length. A velocity field with the initial energy spectrum given by (53) is realized in the simulation by requiring the spectral energy content at each wave number to satisfy (53), but randomly generating the phase and velocity component distributions.³⁰ We also note that when $s=2$, consistency with (15) for a turbulent flow in a box of volume $(2\pi)^3$ requires a uniform mean velocity of random direction with magnitude equal to $\sqrt{B_0}$. However, a uniform velocity has no effect on the computation other than a uniform phase shift of all the Fourier components.

In the simulations with no mean scalar gradient ($\beta=0$), the passive scalar-variance spectrum is initialized analogously to (53). We present results of two simulations with $\beta=0$: the first with an initial energy spectrum with $s=2$ convecting two passive scalar fields with initial spectra having $s'=2$ and 4, and the second with $s=4$ and $s'=2$

and 4. Computations of these two velocity fields and four scalar fields are sufficient to test the previously discussed theoretical results.

In the simulations with a mean scalar gradient ($\beta \neq 0$), the initial fluctuating passive scalar field is taken identically equal to zero, and two simulations are presented with an initial energy spectrum with $s=2$ and $s=4$. The value of β is inconsequential provided it is nonzero, and we choose $\beta=1$.

For later use, we define the large-eddy turnover time $\tau(t)$ as

$$\tau(t) = L_u(t) / \langle u^2 \rangle^{1/2}, \quad (56)$$

where $L_u(t)$ is the velocity integral scale at time t , defined as

$$L_u(t) = \frac{1}{4\pi \langle u^2 \rangle} \int_0^{2\pi} d\phi \int_0^\pi d\psi \sin \psi \int_0^\infty dr \times \langle u_i(\mathbf{x}, t) u_i(\mathbf{x} + \mathbf{r}, t) \rangle = \frac{\pi}{2} \frac{\int_0^\infty k^{-1} E(k, t) dk}{\int_0^\infty E(k, t) dk}, \quad (57)$$

where $\mathbf{r} = (r \sin \psi \cos \phi, r \sin \psi \sin \phi, r \cos \psi)$. For later use, here we also define the scalar integral scale as

$$L_\theta(t) = \frac{1}{4\pi \langle \theta^2 \rangle} \int_0^{2\pi} d\phi \int_0^\pi d\psi \sin \psi \int_0^\infty dr \times \langle \theta(\mathbf{x}, t) \theta(\mathbf{x} + \mathbf{r}, t) \rangle = \frac{\pi}{2} \frac{\int_0^\infty k^{-1} E_\theta(k, t) dk}{\int_0^\infty E_\theta(k, t) dk}. \quad (58)$$

In defining the velocity and scalar integral scales, we have averaged over all the directions of the vector \mathbf{r} and summed over the components of the velocity field. In an isotropic turbulence, L_u is two-thirds the usual longitudinal integral scale typically measured in experiments. We note that the definitions of the integral scales given by (57) and (58) are strictly valid only for an infinite fluid, and must be modified for flow with periodic boundary conditions (see the Appendix).

Use of (53) in (57) and the analogous equations for the scalar-variance spectrum and integral scale yields the following explicit values for the initial integral scales:

$$L_{u,\theta}(0) = \frac{\sqrt{\pi}}{k_p}, \quad s, s' = 2; \quad L_{u,\theta}(0) = \frac{2\sqrt{2\pi}}{3k_p}, \quad s, s' = 4; \quad (59)$$

demonstrating directly that the initial integral scales of the flow are inversely proportional to k_p .

VII. RESULTS FOR DECAYING ISOTROPIC TURBULENCE WITHOUT MEAN SCALAR GRADIENT

The evolution of the energy spectrum with $s=2$ and the associated passive scalar spectra with $s'=2$ and 4 is presented in Fig. 2, and the corresponding spectra for $s=4$ are presented in Fig. 3. The low-wave-number coefficients

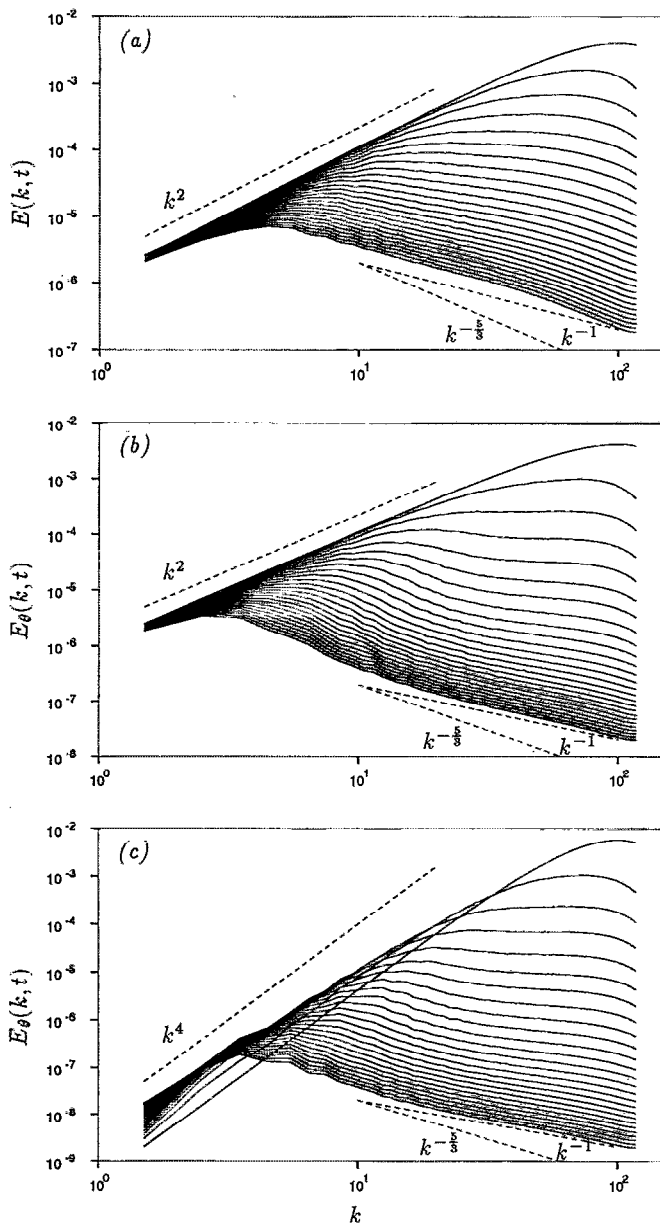


FIG. 2. Time evolution of the spectra with leading-order coefficient B_0 and $\beta=0$: (a) Energy spectrum; (b) scalar-variance spectrum with leading-order coefficient C_0 ; and (c) scalar-variance spectrum with leading-order coefficient C_2 .

of the k^2 spectra are approximately invariant in time (except at the latest times when there is a poor statistical sample of the energetic scales), while the low-wave-number coefficients of the k^4 spectra increase with time, a consequence of nonlinear transfer from small to large scales.

The instantaneous power-law exponents (i.e., the logarithmic time derivatives of the energy and scalar variance) obtained directly from the large-eddy simulations for the decay of $\langle u^2 \rangle$ and $\langle \theta^2 \rangle$ are plotted in Figs. 4 and 5 as a function of $t/\tau(0)$. The solid lines in Figs. 4 and 5 represent the results obtained from the large-eddy simulations and the dashed lines represent the exact and approximate analytical results of Secs. IV and V. The simulation curves

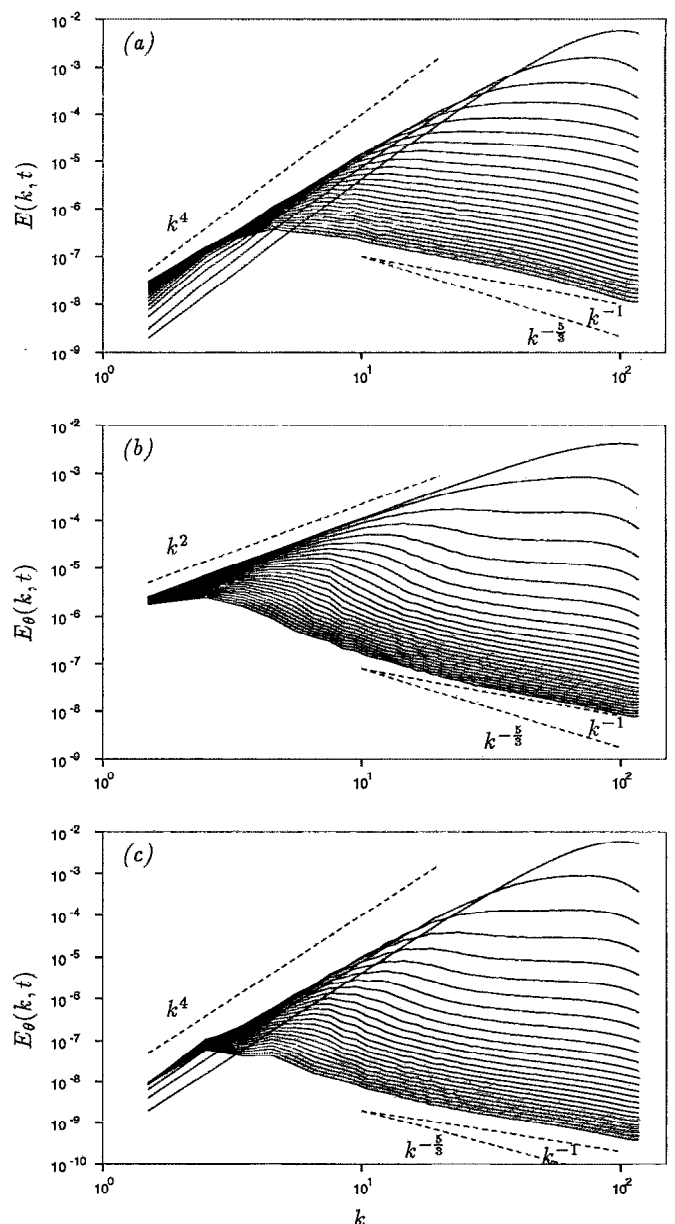


FIG. 3. Time evolution of the spectra with leading-order coefficient B_2 and $\beta=0$: (a) Energy spectrum; (b) scalar-variance spectrum with leading-order coefficient C_0 ; and (c) scalar-variance spectrum with leading-order coefficient C_2 .

are labeled by the leading-order nonzero low-wave-number coefficient of the spectra.

Upon inspection of Figs. 4 and 5, the results of the large-eddy simulations are seen to be in reasonable agreement with the analytical results of Secs. IV and V. In particular, the analytical result $-\frac{5}{3}$ for the decay exponent of $\langle u^2 \rangle$ and $\langle \theta^2 \rangle$ when B_0 and C_0 are the leading-order spectral coefficients is expected to be exact, and we note only a few percent difference between the analytic result and those from the large-eddy simulations.

One observes from Figs. 4 and 5 that the approach of the simulation results to a constant power-law exponent takes a very large number of initial large-eddy turnover times. This is reasonable, since the rate at which the flow

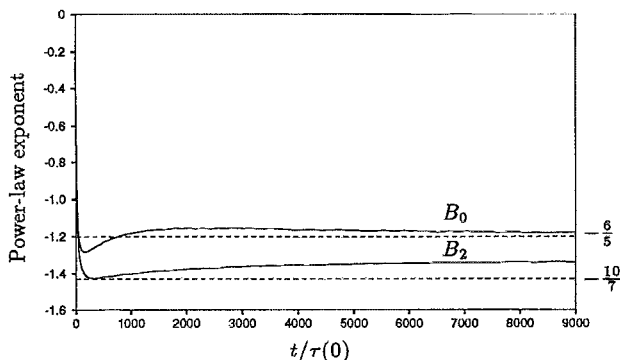


FIG. 4. Time evolution of the power-law exponent of $\langle u^2 \rangle$. The solid lines are the results of the large-eddy simulations and the dashed lines are the exact and approximate analytical results discussed in Secs. IV and V.

approaches its asymptotic state should be governed by the total number of large-eddy turnover times undergone by the flow at time t ,

$$N(t) = \int_0^t \frac{dt'}{\tau(t')}, \quad (60)$$

where $\tau(t)$ is the large-eddy turnover time at time t , and not by the total number of initial large-eddy turnover times, where $\tau(t)$ in (60) is replaced by $\tau(0)$. In an asymptotic similarity state, dimensional arguments yield $\tau(t) \propto t$, so that for large times in the numerical simulations, we have

$$N(t) \propto \ln(t), \quad (61)$$

indicating a slow logarithmic growth in the number of large-eddy turnover times undergone by the flow at time t as a function of t . A plot of $N(t)$ vs $t/\tau(0)$ is presented in Fig. 6 and the slow growth of $N(t)$ at large times is evident.

The slow approach to asymptotic behavior makes it difficult to obtain high precision results from our 256^3 large-eddy simulations for the power-law exponents, since the integral scales of the flow grow to a size comparable to the periodicity length scale before exact attainment of the asymptotic results. This is particularly true for the scalar

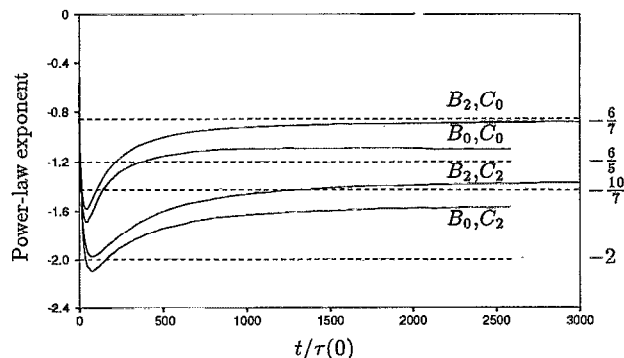


FIG. 5. Time evolution of the power-law exponent of $\langle \theta^2 \rangle$. The solid lines are the results of the large-eddy simulations and the dashed lines are the exact and approximate analytical results discussed in Secs. IV and V.

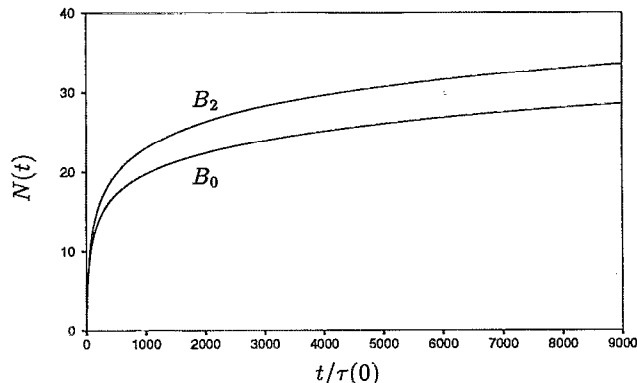


FIG. 6. The number of large-eddy turnover times $N(t)$ undergone by the flow at time $t/\tau(0)$, where $\tau(0)$ is the initial large-eddy turnover time.

decay exponents, because, as we shall see, the integral scale of the scalar field is approximately twice as large as that for the velocity field in the asymptotic similarity state. Simulations performed with the peak of the initial spectra at substantially larger values of k_p would improve the precision of our computations, but must await a new generation of computers. However, lower resolution simulations (128^3) performed with $k_p=50$ do yield similar results to those presented here, indicating that these results are not yet significantly modified by the modeling of an infinite fluid by a periodic flow field.

Another potential source of error in the computed decay exponents plotted in Figs. 4 and 5 is the omission from our calculation of the energy and scalar variance contained in Fourier modes of wave number magnitude greater than k_m . Since we are performing large-eddy simulations, there is still substantial energy and scalar-variance in these sub-grid scales, which conceivably could modify the values of the exponents computed only from the resolved scales. It is indeed possible to include the contribution of the sub-grid scales to the decay exponents by assuming a self-similar evolution for the energy and scalar-variance spectra. If, say, the energy spectrum $E(k)$ has a self-similar form based on some invariant I , one can write, in general,

$$E(k) = I t^{3n/2+1} \hat{E}(\hat{k}), \quad \hat{k} = I^{1/3} t^{n/2+1} k, \quad (62)$$

where n is the true decay exponent of the mean-square velocity. For example, when the energy spectrum has a k^2 form at small k , I is given by $B_0^{3/5}$, and $n = -6/5$. The resolved-scale mean-square velocity in the numerical simulation can be written explicitly as

$$\langle u^2 \rangle_r = I^{2/3} t^n \int_0^{k_m} \hat{E}(\hat{k}) d\hat{k}, \quad (63)$$

so that the time dependence of $\langle u^2 \rangle_r$ is seen to be due to both its explicit dependence on t^n and the dependence of \hat{k}_m on t (k_m being fixed in the simulation). Defining n_r to be the logarithmic derivative of $\langle u^2 \rangle_r$ (this is the quantity plotted in Fig. 4), it follows from (63) that the relationship between n_r and n is given by

$$n_r = n + \frac{t(d/dt) \int_0^{k_m} \hat{E}(\hat{k}) d\hat{k}}{\int_0^{k_m} \hat{E}(\hat{k}) d\hat{k}}. \quad (64)$$

The time derivative of the integral with a time-dependent upper limit may be performed, and the resulting equation may be solved directly for n in terms of n_r to obtain

$$n = \frac{n_r - 2\Delta}{1 + \Delta}, \quad (65)$$

where $\Delta = k_m E(k_m) / \langle u^2 \rangle_r$, corrects the value of n due to the direct effect of the sharp cutoff of the spectrum at k_m . If we assume that $E(k)$ follows the Kolmogorov spectrum at wave number k_m ,

$$E(k_m) \propto \epsilon^{2/3} k_m^{-5/3}, \quad (66)$$

where ϵ is the flux of kinetic energy; then, since by dimensional analysis,

$$\epsilon \propto B_0^{2/5} t^{-11/5}, \quad \epsilon \propto B_2^{2/7} t^{-17/7}, \quad (67)$$

for B_0 and B_2 , the leading spectral coefficients, respectively, Δ decays in time, respectively, as

$$\Delta \propto t^{-4/15}, \quad \Delta \propto t^{-4/21}. \quad (68)$$

For sufficiently long evolution times, the resolved-scale decay exponent will then approach the true decay exponent. At the latest times in our large-eddy simulations, we find approximately a 3% difference between n_r and n for the power-law exponent of the decaying mean-square velocity. For instance, when B_0 is the leading-order energy spectral coefficient, we find the final value $n = -1.215$ to be compared to $n_r = -1.180$. The expected theoretical value is $n = -1.2$.

The assumption of a slow variation in B_2 and C_2 made in Sec. V appears to be quite good in all the computed cases, except perhaps when B_0 and C_2 are the leading-order nonzero coefficients (see Fig. 5), where the error between the approximate analytical result and the resolved-scale LES result is more than 20%. Our EDQNM computation discussed in Sec. V did show that C_2 had a stronger dependence on time when B_0 is the leading-order energy spectrum coefficient than when B_2 is, and this is apparently in qualitative agreement with the simulation results. A LES estimate for the magnitude of the time variation of B_2 and C_2 requires more precise results than that obtained here, although recent simulations of a large ensemble of turbulent flows indicate that $B_2(t) \propto t^\gamma$, with $\gamma \approx 0.25$.³³

In Fig. 7, we present the power-law exponent of the velocity integral scale defined in (57) (also see the Appendix). The power-law exponent of the integral scale for the cases $s=2$ and $s=4$ is observed to be in good agreement with the analytical results.

As a further test of the theoretical ideas of Secs. IV and V, we have rescaled the energy and scalar-variance spectra for the last ten curves in each plot of Figs. 2 and 3 according to their exact and approximate asymptotic similarity forms, and displayed the results in Fig. 8. A good collapse is observed for all the spectra, except perhaps for the scalar

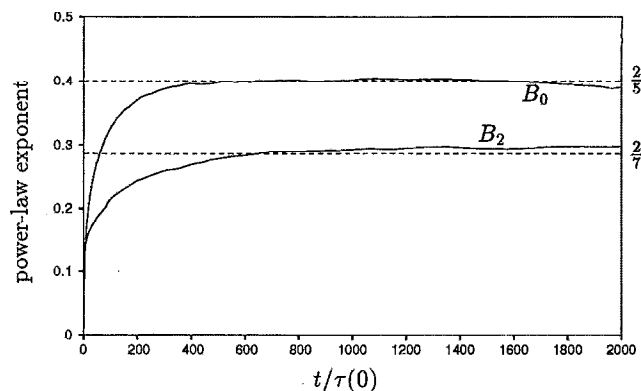


FIG. 7. Time evolution of the power-law exponent of the velocity integral scale. The solid lines are the results of the large-eddy simulations and the dashed lines are the exact and approximate analytical results discussed in Secs. IV and V.

spectrum with leading-order nonzero coefficients B_0 and C_2 . This is consistent with the results for the power-law exponent of $\langle \theta^2 \rangle$ discussed above.

A dimensionless statistic not obtainable by simple dimensional arguments is the ratio of the velocity and scalar integral scales, and this statistic is plotted for the four possible scalar evolutions in Fig. 9. When both the energy and scalar-variance spectra have the same power-law behavior near $k=0$ (be it k^2 or k^4), this ratio takes on an approxi-

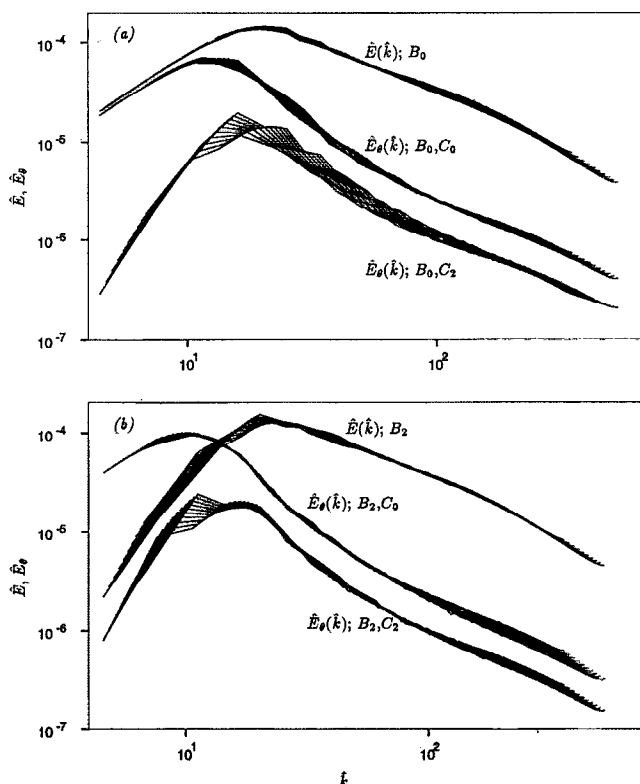


FIG. 8. Rescaling of the last ten spectra in each of Figs. 2 and 3 according to their exact and approximate asymptotic similarity forms given in Secs. IV and V.

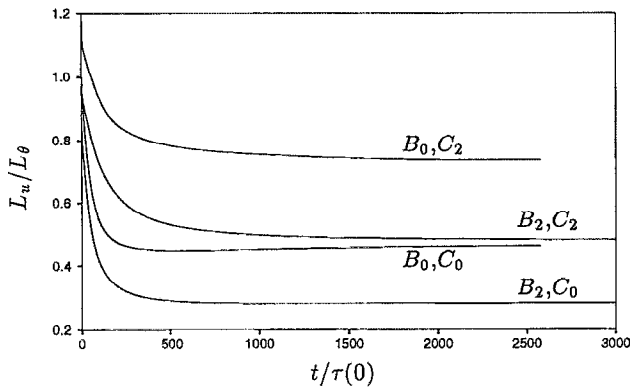


FIG. 9. Time evolution of the ratio of the velocity to scalar integral scales for the four possible scalar evolutions.

mate asymptotic value of $\frac{1}{2}$. In all cases, there is a tendency for the scalar integral scale to become larger than the velocity integral scale. We have earlier noted that this results in less reliable scalar statistics than velocity statistics because of the influence of the periodic boundary conditions.

Here we note that previous large-eddy simulations of decaying isotropic passive scalars^{8,9} found a faster decay of the scalar variance than predicted by the analytical results of Secs. IV and V. This faster decay is also evident in Fig. 5 at small times, where it is observed to be a transient effect. We have further shown that the magnitude of the power-law exponent during this transient is directly related to the initial ratio between the velocity and scalar integral scales, with a larger magnitude when the initial scalar spectrum is peaked at a wave number twice that of the initial energy spectrum, and a smaller magnitude when the initial scalar spectrum is peaked at a wave number half that of the initial energy spectrum. This result is also in qualitative agreement with experiments³ and two-point closure studies.^{5,7}

In a two-point closure Test Field Model (TFM) study,⁷ it was proposed that the power-law exponents, and the integral scales are related by $n_\theta/n_u = 1.63(L_u/L_\theta)^{2/3}$, so that the ratio of the integral scales is determined by

$$\frac{L_u}{L_\theta} = 0.48 \left(\frac{n_\theta}{n_u} \right)^{3/2}, \quad (69)$$

where n_u and n_θ are the power-law exponents of the kinetic energy and scalar variance, respectively. Using the exact and approximate theoretical power-law exponents (see Secs. IV and V) in (69), we exhibit in Table I the TFM predicted values of L_u/L_θ for the four possible asymptotic

TABLE I. Two-point closure (TFM) predicted values of L_u/L_θ compared to the LES results.

	TFM	LES
B_0, C_0	0.48	0.46
B_0, C_2	1.03 (0.74)	0.74
B_2, C_0	0.22	0.30
B_2, C_2	0.48	0.48

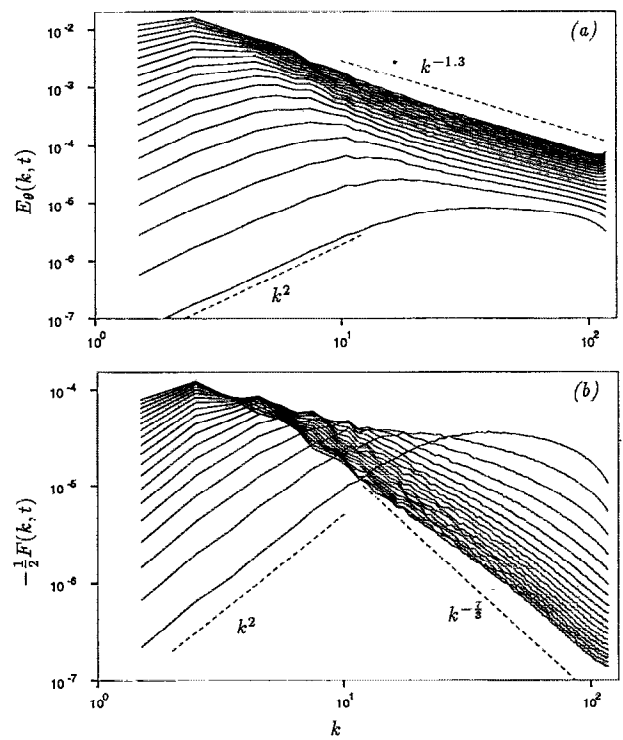


FIG. 10. Time evolution of the spectra with leading-order coefficient B_0 and $\beta=1$: (a) Scalar-variance spectrum; (b) scalar-flux spectrum.

similarity states, and compare them to the integral scale ratios obtained from our LES results (see Fig. 9). Because of the large discrepancy between the approximate theoretical decay exponent and the LES result when the leading-order spectral coefficients are B_0 and C_2 , we have added in parentheses the integral scale ratio predicted by (69) when the LES exponent $n_\theta = -1.6$ is used, instead of the approximate theoretical result $n_\theta = -2$. Even though (69) was developed only for the particular case of B_2 and C_2 being the leading-order spectral coefficients, the agreement between (69) and the four ratios obtained from the LES results is quite good.

VIII. RESULTS FOR A PASSIVE SCALAR WITH MEAN SCALAR GRADIENT

In Figs. 10 and 11 we plot the time evolution of the scalar-variance spectrum and the scalar-flux spectrum in the presence of a uniform passive mean-scalar gradient ($\beta = 1$). Both spectra increase from initially zero values.

In Fig. 12, we plot the power-law exponent of the resolved scale $\langle \theta^2 \rangle$ as a function of $t/\tau(0)$. The solid lines are the simulation results and the dashed lines are the analytical results found in Secs. IV and V. The analytic result when B_0 is the leading-order nonzero coefficient is expected to be exact, and here we find good agreement with the large-eddy simulation results. Reasonable agreement between the simulation and the approximate analytical result is found for the case when B_2 is the leading-order coefficient. In Fig. 13, we rescale the last ten scalar-variance and scalar-flux spectra shown in Figs. 10 and 11

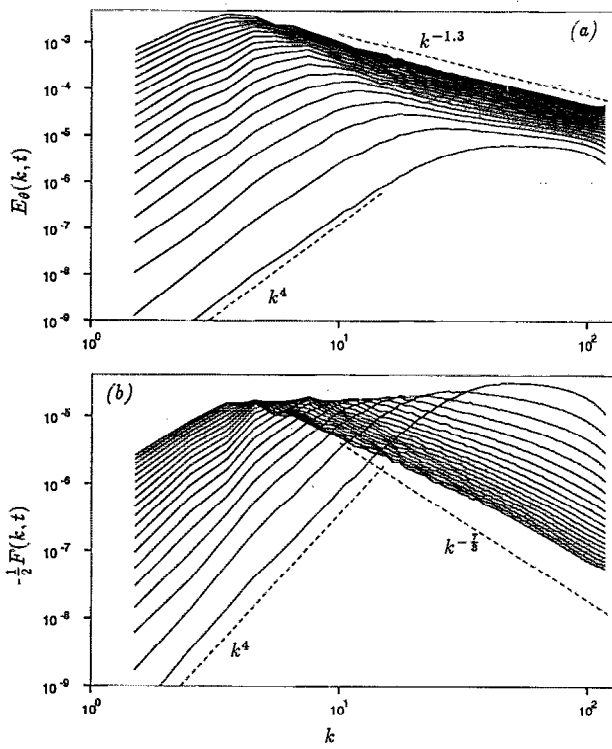


FIG. 11. Time evolution of the spectra with leading-order coefficient B_2 and $\beta=1$: (a) Scalar-variance spectrum; (b) scalar-flux spectrum.

according to their exact and approximate asymptotic similarity forms presented in (31) and (32) and (44) and (45). A good collapse is observed, providing further evidence for the existence of a similarity state.

In Fig. 14, we plot the ratio of the velocity to scalar spherically averaged integral scale in this flow. Again, we note that the scalar integral scale is larger than the velocity integral scale in the final similarity state, although here the factor is closer to $\frac{2}{3}$ than $\frac{1}{2}$. The scalar integral scale also has a different value along different directions in this flow because of the direction singled out by the mean scalar gradient. In Fig. 15, we plot the ratio of the scalar integral scale taken along the mean scalar gradient to that taken

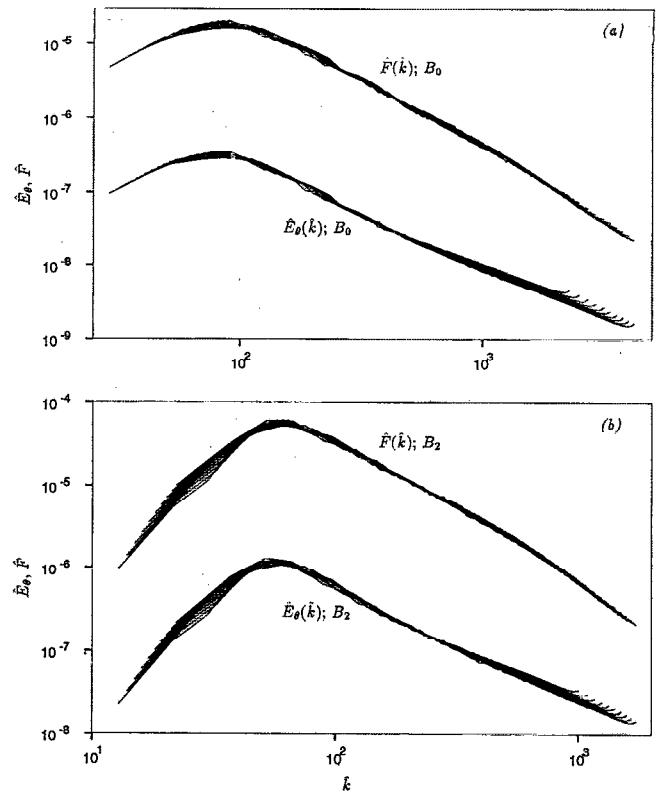


FIG. 13. Rescaling of the last ten spectra in each of Figs. 10 and 11 according to their exact and approximate asymptotic similarity forms given in Secs. IV and V.

perpendicular to the gradient. Immediately after the initial generation of scalar fluctuations this ratio is exactly two, whereas at later times nonlinear effects decrease this ratio to about 1.4.

Sirivat and Warhaft⁴ measured in their laboratory experiment the ratio between the scalar integral scale in the direction perpendicular to the gradient and the longitudinal velocity integral scale, and obtained a value of 0.9. From our simulation data, we find a value closer to 0.8 when B_2 is the leading-order spectral coefficient, and slightly lower when B_0 is the leading-order coefficient.

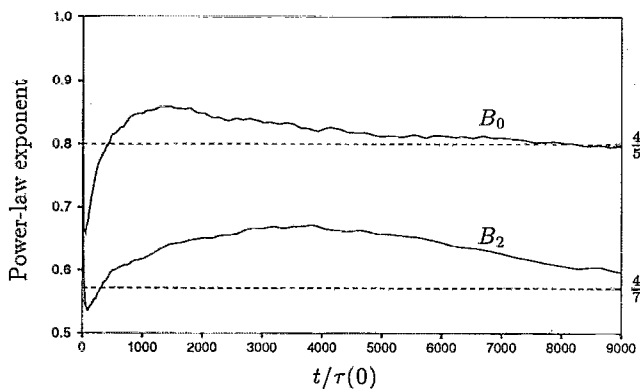


FIG. 12. Time evolution of the power-law exponent of $\langle \theta^2 \rangle$ for decaying isotropic turbulence with a passive mean scalar gradient.

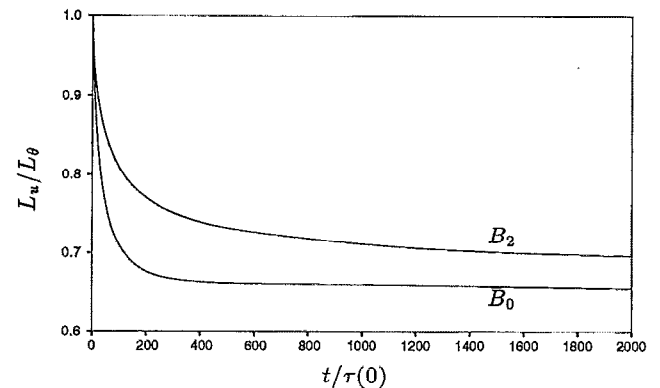


FIG. 14. Time evolution of the ratio of the velocity to scalar integral scales for the two possible scalar evolutions.

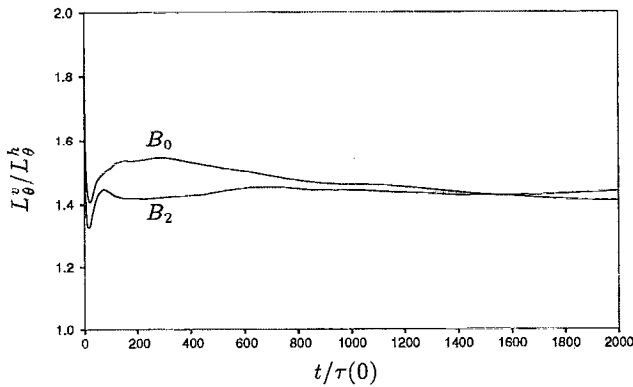


FIG. 15. Time evolution of the ratio of the scalar integral scale taken along the gradient L_θ^b to that taken perpendicular to the gradient L_θ^a .

Another nondimensional quantity measurable in this flow is the normalized correlation coefficient between the scalar field and the vertical velocity fluctuation ρ , defined in (22). Immediately following the initial generation of scalar fluctuations $\rho=1$, whereas for isotropic passive scalars $\rho=0$ for all times. In Fig. 16 we plot ρ as a function of $t/\tau(0)$. As the flow evolves, nonlinear effects are seen to decorrelate the scalar and third component of the velocity field until ρ attains the approximate asymptotic value of 0.7 when B_0 is the leading-order spectral coefficient, and slightly lower when B_2 is the leading-order coefficient. This value is in good agreement with the experimental value of 0.7 found earlier by Sirivat and Warhaft.⁴

In addition, Sirivat and Warhaft obtained asymptotic experimental results for the ratio of the scalar-variance production to dissipation, $-\beta\langle u_3\theta \rangle/\epsilon_\theta$, and the mechanical to scalar time-scale ratio $(\langle u^2 \rangle/\epsilon)/(\langle \theta^2 \rangle/\epsilon_\theta)$, where ϵ and ϵ_θ is the kinetic energy and one-half scalar-variance dissipation rates, respectively. The time evolution of these two ratios from the large-eddy simulation is displayed in Fig. 17. Sirivat and Warhaft obtain a value of 1.5 for the ratio of the scalar-variance production to dissipation and we find asymptotic values of approximately 1.6 and 1.4 when B_0 and B_2 are the leading-order spectral coefficients, respectively. For the mechanical to scalar time-scale ratio,

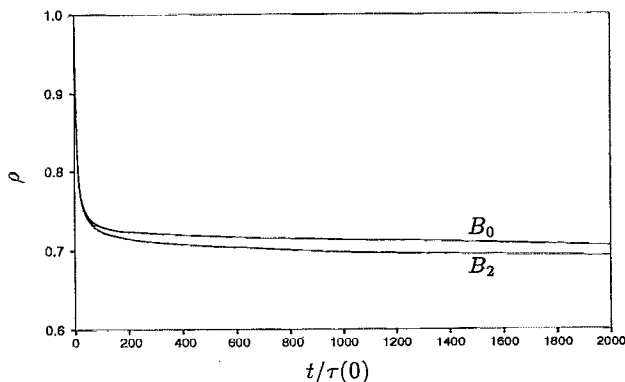


FIG. 16. Time evolution of the normalized correlation coefficient between the scalar field and the vertical velocity fluctuation.

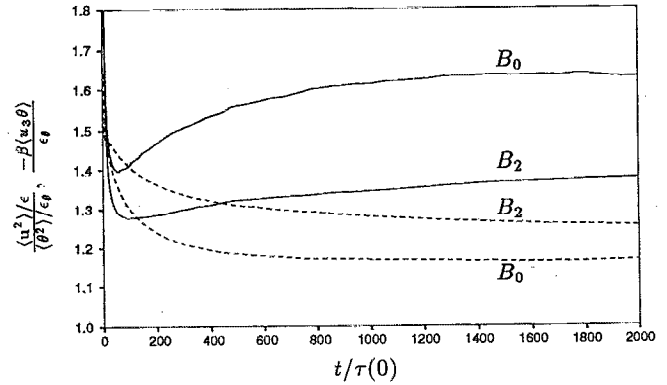


FIG. 17. Time evolution of the ratio of the scalar-variance production to dissipation (—), and the mechanical to scalar time scale (---).

Sirivat and Warhaft obtain the value 1.4, although there is considerable scatter in their data, and we find values of 1.15 and 1.25, respectively. We also note that the following theoretical relationship exists between these two ratios:

$$\frac{\langle u^2 \rangle/\epsilon}{\langle \theta^2 \rangle/\epsilon_\theta} = \frac{n_\theta}{n_u} \left(1 + \frac{\beta\langle u_3\theta \rangle}{\epsilon_\theta} \right)^{-1}, \quad (70)$$

where n_u and n_θ are the time exponents of the kinetic energy and scalar variance.

IX. SMALL-SCALE SPECTRA

All of the results presented above have been based on the large-scale structure of homogeneous turbulence and its consequences for the energy and scalar-variance containing range of eddies. Here we will examine some of the spectral results of our simulations with regard to the small-scale turbulence.

A similarity state of the small-scale statistics of the velocity field, which depends only on the rate of energy dissipation ϵ , and the kinematic viscosity ν was originally proposed by Kolmogorov.³⁴ An analogous similarity state of the small-scale statistics of a passive scalar field, which also depends on the rate of (one-half) scalar-variance dissipation ϵ_θ , and the molecular diffusivity D was proposed independently by Obukhov³⁵ and Corrsin.³⁶ The existence of a similarity state for passive scalar transport in isotropic turbulence based on the low-wave-number spectral coefficients implies that ϵ and ϵ_θ themselves are functions of these coefficients, and time t . We have so expressed ϵ in (67) above, and ϵ_θ may also be given by one of

$$\begin{aligned} \epsilon_\theta &\propto C_0 B_0^{-3/5} t^{-11/5}, & \epsilon_\theta &\propto C_2 B_0^{-1} t^{-3}, \\ \epsilon_\theta &\propto C_0 B_2^{-3/7} t^{-13/7}, & \epsilon_\theta &\propto C_2 B_2^{-5/7} t^{-17/7}, \end{aligned} \quad (71)$$

in the absence of a mean scalar gradient. In the presence of a mean scalar gradient, ϵ_θ is given by one of

$$\epsilon_\theta \propto \beta^2 B_0^{2/5} t^{-1/5}, \quad \epsilon_\theta \propto \beta^2 B_2^{2/7} t^{-3/7}. \quad (72)$$

Although ϵ and ϵ_θ depend on large-scale properties of the flow, as demonstrated explicitly by (67), (71), and (72), the essence of the Kolmogorov hypothesis, and its scalar field analog is that the statistics of scales lying in an

inertial-convective subrange may depend on the energy and scalar-variance containing scales of the flow only through ϵ and ϵ_θ . The celebrated $k^{-5/3}$ power laws for the energy and scalar-variance spectra in the inertial-convective subrange are then obtained by assuming molecular transport coefficients are irrelevant for these scales, so that by dimensional analysis,

$$E(k) \propto \epsilon^{2/3} k^{-5/3}, \quad E_\theta(k) \propto \epsilon_\theta \epsilon^{-1/3} k^{-5/3}. \quad (73)$$

Here we present a simple argument for the form of the scalar-flux spectrum $F(k)$ in the inertial-convective subrange. A scaling for $F(k)$ based solely on ϵ and ϵ_θ is unsatisfactory, since $F(k)$ must vanish when the scalar statistics are isotropic, as occurs when $\beta=0$. From the governing equation (3) for the scalar field it is evident that θ depends linearly on the mean scalar gradient β when β is nonzero. Accordingly, we postulate the scaling

$$F(k) = \beta f(\epsilon, \epsilon_\theta, k), \quad (74)$$

for wave numbers lying in the inertial-convective subrange. Although it is true that ϵ_θ itself is a quadratic function of β when β is nonzero, we emphasize again that this is of no importance under a Kolmogorov-like hypothesis since ϵ_θ itself is taken as the fundamental variable. Dimensional analysis applied to (74) yields, directly,

$$F(k) \propto \beta \epsilon^{1/3} k^{-7/3}. \quad (75)$$

Hence the scalar-flux spectrum $F(k)$ decreases faster than $\sqrt{E(k)E_\theta(k)}$ with increasing k , as is reasonable for a return to isotropy of the small scales. Here we note that the same $k^{-7/3}$ spectrum for $F(k)$ has been previously predicted for a stably stratified flow.³⁷ An analogous derivation of the buoyancy-flux spectrum for homogeneous buoyancy generated turbulence may be given,³⁸ and in this flow the buoyancy-flux spectrum also follows a $k^{-7/3}$ law, but with a different scaling coefficient seen to be directly proportional to the gravitational acceleration g rather than the scalar gradient β .

The small-scale wave-number power-law exponents evident in Figs. 2 and 3 and 10 and 11 show some anomalous behaviors with respect to the above scaling laws, (73) and (75). In particular, the passive scalar field without a mean-scalar gradient has a strong tendency toward a k^{-1} spectrum, as previously noted,⁸ whereas in the presence of a scalar gradient, the tendency of the scalar-variance spectrum is toward an exponent of approximately $k^{-1.3}$. The scalar-flux spectrum is also apparently somewhat less steep than the $k^{-7/3}$ spectrum predicted above. It is difficult for us to judge the influence of the subgrid scale model on these spectral exponents, but we note that an approximate k^{-1} scalar spectral slope has also been observed in direct numerical simulations.⁹

Nevertheless, despite the deviations from the classical power-law exponents above, we can still try to collapse our small-scale spectra according to the above scalings. In particular, we plot the compensated spectra,

$$k^{5/3} E(k) / \epsilon^{2/3}, \quad k^{5/3} \epsilon^{1/3} E_\theta(k) / \epsilon_\theta, \quad k^{7/3} F(k) / \beta \epsilon^{1/3}$$

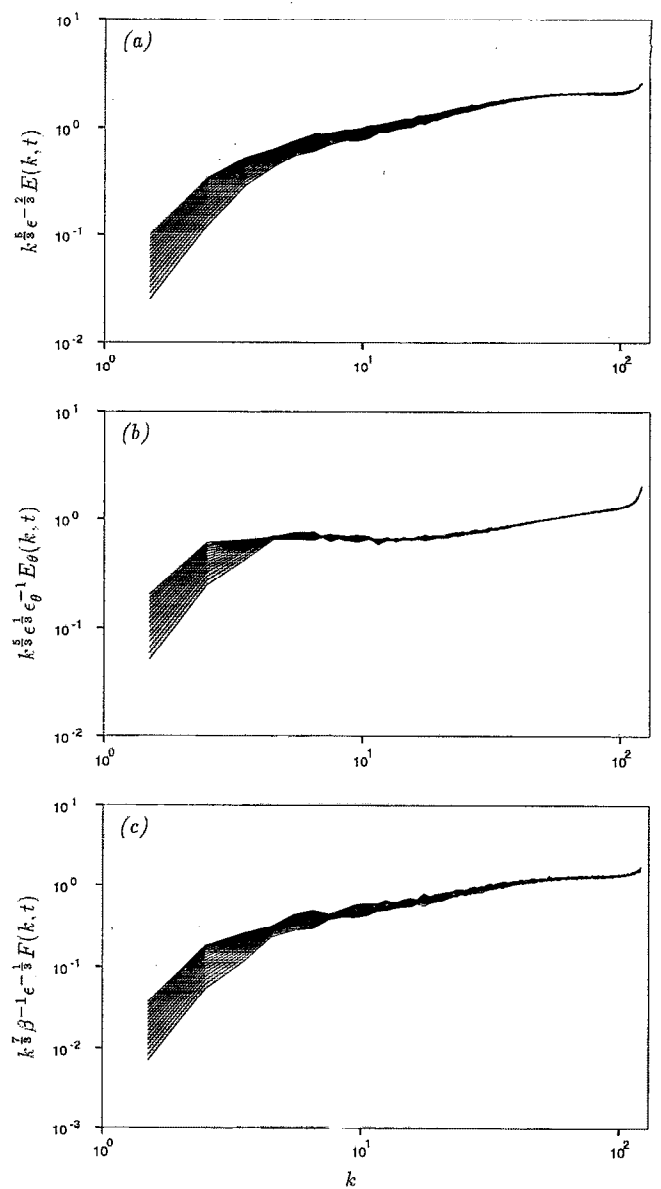


FIG. 18. Compensated spectra with leading-order coefficient B_0 and $\beta=1$: (a) energy spectrum; (b) scalar-variance spectrum; and (c) scalar-flux spectrum.

vs k for our large-eddy simulations of decaying isotropic turbulence in a passive scalar gradient with nonzero B_0 in Fig. 18. Although the k power-law exponents are not well followed, the spectra still collapse at the highest wave numbers, lending at least partial support to the classical scalings. We do not know why the power-law exponents are not well reproduced, although closure studies¹⁰ indicate that inertial-convective range asymptotics may be difficult to obtain from numerical simulations of limited wave number span.

X. CONCLUSIONS

Simple analytical arguments with a minimum number of assumptions have been shown to yield the asymptotic long-time, high Reynolds and Péclet number decay laws of the kinetic energy and scalar variance in a decaying isotro-

pic turbulence with decaying isotropic passive scalars. These laws were previously derived by assuming a similarity state for the energy and scalar-variance spectra.¹³ We show that, in fact, the only necessary assumption is that the energy and scalar variance depend asymptotically on invariants of the velocity and scalar field; self-similarity of the spectra follows directly from this assumption. A plausibility argument is offered for this asymptotic scaling by comparing flow at high Reynolds numbers to that during the final period, for which exact solutions may be obtained.

We have also determined the high Reynolds and Péclet number similarity state for a passive scalar in the presence of a uniform mean scalar gradient. Here, the scaling is based only on an invariant of the velocity field. The scalar variance is found to increase in this similarity state, in agreement with earlier experimental results. We further determine that the scalar variance may increase or decrease in the final period, depending on the form of the low-wave-number energy spectrum. This exact analytical result may be of use in the determination of the form of the low-wave-number energy spectrum in grid-generated turbulence experiments.

Decaying isotropic turbulence in the presence of a uniform passive scalar gradient can be seen to be mathematically analogous to buoyancy-generated turbulence studied earlier,¹⁴ but with the roles played by the fluctuating velocity and scalar fields reversed, and the mean scalar gradient replacing the constant gravitational acceleration. In the buoyancy-generated flow, it is the low-wave-number coefficient of the scalar-variance spectrum that is invariant, and the similarity state that develops is based on this invariant.

Finally, large-eddy simulations of a high Reynolds and Péclet number flow were performed to test the theoretical predictions. These large-eddy simulations are similar to earlier work,^{8,9} but here the fields are evolved sufficiently far in time to observe the development of an asymptotic similarity state. Power-law exponents of the kinetic energy, scalar variance, and velocity integral scale were determined and shown to support the analytical results. Additional statistics—such as the ratio of the velocity to scalar integral scale, the ratio of the scalar integral scale taken along the mean scalar gradient to that taken perpendicular to the gradient, the normalized correlation coefficient between the scalar field and the vertical velocity fluctuation, the ratio of the scalar-variance production to dissipation, and the ratio of the mechanical to scalar time scale—were computed and compared to existing experimental data and two-point closure studies. The analytical and numerical methods exploited in this work are currently being extended to other homogeneous flows.

ACKNOWLEDGMENTS

I wish to thank Professor M. Lesieur for his hospitality and support of this work during my half-year visit to his laboratory in Grenoble and Dr. R. Rogallo for providing me his numerical simulation code and for many interesting discussions. I am also grateful to Professor G. K. Batchelor

for detailed discussions on this work, and to Dr. O. Metais, Dr. J. Riley, and Dr. N. Mansour for their helpful comments. I also wish to express my appreciation to Professor P. Moin and Professor W. Reynolds for providing me the opportunity to pursue this research at CTR. The simulations in this paper were performed on the NASA-Ames Cray YMP, the NAS 128 node Intel hypercube, and the Caltech 512 node Intel machine, and I gratefully acknowledge the support of these institutions. The vectorial language compilers for the YMP and the Intel machines were written by Dr. A. Wray. This work was partially supported by a scholarship from the French government while I was a visitor at the Institut de Mécanique de Grenoble.

APPENDIX: COMPUTATION OF THE INTEGRAL SCALE IN A PERIODIC FLOW

Equation (57) defines the spherically-averaged velocity integral scale in an infinite fluid. Our simulation approximates an infinite fluid by a velocity field that is periodic within a cube of length 2π . The analogous definition for the integral scale in the periodic flow is

$$L_u(t) = \frac{1}{\langle u^2 \rangle} \int_V \frac{\langle u_i(\mathbf{x}, t) u_i(\mathbf{x} + \mathbf{r}, t) \rangle}{4\pi r^2} d\mathbf{r}, \quad (\text{A1})$$

where we restrict the integration region to the volume of a sphere of radius π lying completely inside a single periodic box of length 2π . Such a spherically averaged integral scale will have less statistical error than an integral scale which is computed by only averaging over the three periodic directions of the flow, as is customary.

To compute (A1), the velocity field may be expanded in a Fourier series as

$$\mathbf{u}(\mathbf{x}, t) = \sum_{\mathbf{k}} \hat{\mathbf{u}}(\mathbf{k}, t) \exp(i\mathbf{k} \cdot \mathbf{x}), \quad (\text{A2})$$

where the components of \mathbf{k} in the sum span the set of integers. Replacing the ensemble average in (A1) by a volume average over the entire periodic box, and substituting the Fourier expansion (A2) into (A1), we obtain, after integrating over the box,

$$L_u(t) = \frac{1}{4\pi \langle u^2 \rangle} \sum_{\mathbf{k}} \hat{u}_i(\mathbf{k}, t) \hat{u}_i(-\mathbf{k}, t) \int_V \frac{\exp(i\mathbf{k} \cdot \mathbf{r})}{r^2} d\mathbf{r}. \quad (\text{A3})$$

The remaining integral over a sphere of radius π may be most easily performed in spherical coordinates, and we obtain

$$L_u(t) = \frac{\pi |\hat{\mathbf{u}}(0, 0, 0)|^2}{\langle u^2 \rangle} + \frac{\pi}{2 \langle u^2 \rangle} \times \sum_{\mathbf{k} \neq 0} \frac{\hat{u}_i(\mathbf{k}, t) \hat{u}_i(-\mathbf{k}, t)}{k} \left(\frac{2}{\pi} \text{Si}(\pi k) \right), \quad (\text{A4})$$

where k is the magnitude of the wave vector \mathbf{k} , $\langle u^2 \rangle$ may be computed from the Fourier coefficients as

$$\langle u^2 \rangle = \sum_{\mathbf{k}} \hat{u}_i(\mathbf{k}, t) \hat{u}_i(-\mathbf{k}, t)$$

and

$$\text{Si}(x) = \int_0^x \frac{\sin(y)}{y} dy.$$

The Fourier coefficient $\hat{u}(0,0,0)$ is equal to the uniform velocity of the fluid in the periodic box; the maximum value possible for L_u is π , and this value is attained when $\hat{u}(0,0,0)$ is the only nonzero Fourier coefficient. The first term on the right side of (A3) is identically zero when B_2 is the leading-order spectral coefficient, and, although nonzero when B_0 is the leading-order coefficient, may be safely neglected in our simulations. The quantity in large parentheses in (A4) approaches unity for large values of πk , as it must, in order to recover (57) for an infinite fluid. In our simulations where the integral scale is much smaller than π , it may be safely set to unity when B_2 is the leading-order spectral coefficient, but has a few percent effect on our results when B_0 is the leading-order coefficient. To implement (A4) in the simulation, we have used a highly accurate rational approximation³⁹ for $\text{Si}(x)$.

Analogous results may be obtained for the scalar integral scale $L_\theta(t)$.

- ¹G. Comte-Bellot and S. Corrsin, "The use of a contraction to improve the isotropy of a grid generated turbulence," *J. Fluid Mech.* **25**, 657 (1966).
- ²T. T. Yeh and C. W. Van Atta, "Spectral transfer of scalar and velocity fields in heated-grid turbulence," *J. Fluid Mech.* **58**, 233 (1973).
- ³Z. Warhaft and J. L. Lumley, "An experimental study of the decay of temperature fluctuations in grid-generated turbulence," *J. Fluid Mech.* **88**, 659 (1978).
- ⁴A. Sivrat and Z. Warhaft, "The effect of a passive cross-stream temperature gradient on the evolution of temperature variance and heat flux in grid turbulence," *J. Fluid Mech.* **128**, 323 (1983).
- ⁵M. Larcheveque, J. P. Chollet, J. R. Herring, M. Lesieur, G. R. Newman, and D. Schertzer, "Two-point closure applied to a passive scalar in decaying isotropic turbulence," in *Turbulent Shear Flows II*, edited by J. S. Bradbury, F. Durst, B. E. Launder, F. W. Schmidt, and J. H. Whitelaw (Springer-Verlag, Berlin, 1980), pp. 50–65.
- ⁶M. Nelkin and R. M. Kerr, "Decay of scalar variance in terms of a modified Richardson law for pair dispersion," *Phys. Fluids* **24**, 1754 (1981).
- ⁷J. R. Herring, D. Schertzer, M. Lesieur, G. R. Newman, J. P. Chollet, and M. Larcheveque, "A comparative assessment of spectral closures as applied to passive scalar diffusion," *J. Fluid Mech.* **124**, 411 (1982).
- ⁸M. Lesieur and R. S. Rogallo, "Large-eddy simulation of passive scalar diffusion in isotropic turbulence," *Phys. Fluids A* **1**, 718 (1989).
- ⁹O. Metais and M. Lesieur, "Spectral large-eddy simulation of isotropic and stably stratified turbulence," *J. Fluid Mech.* **239**, 157 (1992).
- ¹⁰J. R. Herring, "Comparison of closure to the spectral-based large eddy simulations," *Phys. Fluids A* **2**, 979 (1990).
- ¹¹S. Corrsin, "Heat transfer in isotropic turbulence," *J. Appl. Phys.* **23**, 113 (1952).
- ¹²R. C. Sanderson, A. D. Leonard, and J. C. Hill, "Turbulent transport of a passive scalar," in *Proceedings of the 12th Rolla Symposium on Turbulence*, 1990.
- ¹³M. Lesieur, *Turbulence in Fluids* (Kluwer, Dordrecht, 1990).
- ¹⁴G. K. Batchelor, V. M. Canuto, and J. R. Chasnov, "Homogeneous buoyancy-generated turbulence," *J. Fluid Mech.* **235**, 349 (1992).
- ¹⁵G. K. Batchelor, "Energy decay and self-preserving correlation functions in isotropic turbulence," *Quart. Appl. Math.* **6**, 97 (1948).
- ¹⁶G. K. Batchelor, *The Theory of Homogeneous Turbulence* (Cambridge U.P., Cambridge, 1953).
- ¹⁷G. K. Batchelor and I. Proudman, "The large-scale structure of homogeneous turbulence," *Philos. Trans. R. Soc. London* **248**, 369 (1956).
- ¹⁸P. G. Saffman, "The large-scale structure of homogeneous turbulence," *J. Fluid Mech.* **27**, 581 (1967).
- ¹⁹S. Corrsin, "The decay of isotropic temperature fluctuations in an isotropic turbulence," *J. Aeronaut. Sci.* **18**, 417 (1951).
- ²⁰D. W. Dunn and W. H. Reid, "Heat transfer in isotropic turbulence during the final period of decay," *NACA TN* 4186, 1958.
- ²¹G. K. Batchelor and A. A. Townsend, "Decay of turbulence in the final period," *Proc. R. Soc. London Ser. A* **194**, 527 (1948).
- ²²J. C. Bennett and S. Corrsin, "Small Reynolds number nearly isotropic turbulence in a straight duct and a contraction," *Phys. Fluids* **21**, 2129 (1978).
- ²³P. G. Saffman, "Note on decay of homogeneous turbulence," *Phys. Fluids* **10**, 1349 (1967).
- ²⁴A. N. Kolmogorov, "On degeneration of isotropic turbulence in an incompressible viscous liquid," *Dokl. Akad. Nauk. SSSR* **31**, 538 (1941).
- ²⁵L. G. Loitsianski, "Some basic laws for isotropic turbulent flow," *Trudy Tsentr. Aero. Giedrodin. Inst.* **440**, 31 (1939).
- ²⁶C. C. Lin, "Remarks on the spectrum of turbulence," *Proceedings of the 1st Symposium on Applied Mathematics*, 1947, p. 81.
- ²⁷M. Lesieur and D. Schertzer, "Amortissement auto similaire d'une turbulence a grand nombre de Reynolds," *J. Mec.* **17**, 609 (1980).
- ²⁸J. P. Chollet, These de Doctorat d'Etat, Grenoble, 1983.
- ²⁹C. G. Speziale and P. S. Bernard, "The energy decay in self-preserving isotropic turbulence revisited," *J. Fluid Mech.* **241**, 645 (1992).
- ³⁰R. S. Rogallo, "Numerical experiments in homogeneous turbulence," *NASA TM* 81315, 1981.
- ³¹R. H. Kraichnan, "Eddy viscosity in two and three dimensions," *J. Atmos. Sci.* **33**, 1521 (1976).
- ³²J. P. Chollet and M. Lesieur, "Parameterization of small scales of three-dimensional isotropic turbulence utilizing spectral closures," *J. Atmos. Sci.* **38**, 2747 (1981).
- ³³J. R. Chasnov, "Computation of the Loitsianski integral in decaying isotropic turbulence," *Phys. Fluids A* **5**, 2579 (1993).
- ³⁴A. N. Kolmogorov, "The local structure of isotropic turbulence at very high Reynolds numbers," *Compt. Rend. Acad. Sci. URSS* **30**, 301 (1941).
- ³⁵A. M. Obukhov, "Structure of the temperature field in turbulent flows," *Isv. Geogr. Geophys. Ser.* **13**, 58 (1949).
- ³⁶S. Corrsin, "On the spectrum of isotropic temperature fluctuations in an isotropic turbulence," *J. Appl. Phys.* **22**, 469 (1951).
- ³⁷J. L. Lumley, "The spectrum of nearly inertial turbulence in a stably stratified fluid," *J. Atmos. Sci.* **21**, 99 (1964).
- ³⁸J. R. Chasnov, "Local isotropy in buoyancy-generated turbulence," *Annual Research Briefs* (Center for Turbulence Research, Stanford, CA, 1991), 1991, pp. 21–29.
- ³⁹M. Abramowitz and I. A. Stegun, *Handbook of Mathematical Functions* (Dover, New York, 1965), p. 233.